Mon. Not. R. Astron. Soc. **359,** 1537–1548 (2005) doi:10.1111/j.1365-2966.2005.09020.x

Dark matter subhaloes in numerical simulations

Darren Reed,[1★] Fabio Governato,[2,3] Thomas Quinn,[2] Jeffrey Gardner,[4] Joachim Stadel[5] and George Lake[6]

[1] *Institute for Computational Cosmology, Department of Physics, University of Durham, South Road, Durham DH1 3LE*
[2] *Astronomy Department, Box 351580, University of Washington, Seattle, WA 98195, USA*
[3] *INAF, Osservatorio Astronomico di Brera, via Brera 28, I-20131 Milano, Italy*
[4] *Pittsburgh Supercomputing Centre, 4400 Fifth Avenue, Pittsburgh, PA 15213, USA*
[5] *Institute for Theoretical Physics, University of Zurich, Winterthurerstrasse 190, Zurich 8057, Switzerland*
[6] *Department of Physics, Washington State University, PO Box 642814, Pullman, WA 99164, USA*

Accepted 2005 March 4. Received 2005 February 21; in original form 2004 June 3

ABSTRACT

We use cosmological Λ cold dark matter (CDM) numerical simulations to model the evolution of the substructure population in 16 dark matter haloes with resolutions of up to seven million particles within the virial radius. The combined substructure circular velocity distribution function (VDF) for hosts of 10^{11} to $10^{14}\,\mathrm{M}_{\odot}$ at redshifts from zero to two or higher has a self-similar shape, is independent of host halo mass and redshift, and follows the relation $\mathrm{d}n/\mathrm{d}v = (1/8)(v_{\mathrm{cmax}}/v_{\mathrm{cmax,host}})^{-4}$. Halo to halo variance in the VDF is a factor of roughly 2 to 4. At high redshifts, we find preliminary evidence for fewer large substructure haloes (subhaloes). Specific angular momenta are significantly lower for subhaloes nearer the host halo centre where tidal stripping is more effective. The radial distribution of subhaloes is marginally consistent with the mass profile for $r \gtrsim 0.3 r_{\mathrm{vir}}$, where the possibility of artificial numerical disruption of subhaloes can be most reliably excluded by our convergence study, although a subhalo distribution that is shallower than the mass profile is favoured. Subhalo masses but not circular velocities decrease towards the host centre. Subhalo velocity dispersions hint at a positive velocity bias at small radii. There is a weak bias towards more circular orbits at lower redshift, especially at small radii. We additionally model a cluster in several power-law cosmologies of $P \propto k^n$, and demonstrate that a steeper spectral index, n, results in significantly less substructure.

Key words: methods: *N*-body simulations – galaxies: formation – galaxies: haloes – cosmology: theory – dark matter.

1 INTRODUCTION

A critical test of the Λ cold dark matter (CDM) model is its ability to accurately predict the evolution of the distribution of subhaloes within dark matter haloes, or haloes within haloes. The hierarchical formation process of CDM haloes by multiple mergers (White & Rees 1978) leaves behind tidally stripped merger remnants that survive as bound subhaloes within larger haloes (Ghigna et al. 1998). Subhaloes serve as hosts for visible galaxies within clusters, groups, or larger galaxies, and so provide a powerful and observable cosmological probe. In cases where dark matter subhaloes may have no luminous counterparts, the substructure population can be inferred from gravitational lensing studies (e.g. Mao & Schneider 1998; Metcalf & Madau 2001; Chiba 2002; Dalal & Kochanek 2002; Mao et al. 2004).

CDM models predict the abundance of substructure to be roughly self-similar, independent of halo mass (Klypin et al. 1999; Moore et al. 1999) and to follow a Poisson distribution (Kravtsov et al. 2004a). Subhalo numbers predicted by the ΛCDM model are reasonably matched by observations of clusters (Ghigna et al. 2000; Springel et al. 2001; Desai et al. 2004; see however Diemand, Moore & Stadel 2004b). However, observations measure roughly an order of magnitude fewer subhaloes in Galactic haloes than in clusters (Klypin et al. 1999; Moore et al. 1999). Thus, mass is either more smoothly distributed on small scales than predicted by ΛCDM cosmology, or Galactic dark matter subhaloes are poorly traced by stars. An element of uncertainty in the comparisons with ΛCDM model predictions is the possibility of significant halo to halo variation in the subhalo population that could depend on host mass, merging history, or environment. Results from the handful of

★E-mail: d.s.reed@durham.ac.uk

high-resolution simulations on galactic scales to date suggest that such variance in substructure numbers is significant but much too small to account for the apparent discrepancy in Galactic subhaloes (e.g. Klypin et al. 1999; Moore et al. 1999; Font et al. 2001). Even if observed Galactic dwarfs reside in subhaloes of significantly deeper potential than inferred from their stellar velocity dispersions and radial extent, which could allow the most massive satellites to match predictions (Stoehr et al. 2002; Hayashi et al. 2003; however see also Kazantzidis et al. 2004; Willman et al. 2004), then the non-detection of the vast majority of small subhaloes remains an unsolved problem. However, semi-analytic work suggests that baryonic physics causes small haloes to remain starless, indicating that observations may be consistent with the ΛCDM model (e.g. Bullock, Kravtsov & Weinberg 2000; Benson et al. 2002a,b; Somerville 2002).

By analysing substructure in a large number of dark matter haloes, we can measure the range of halo to halo variation and better constrain the uncertainty in the ΛCDM subhalo distribution with the improved statistics. With better numerical resolution and a broad range in host halo masses, substructure can be used to place cosmological constraints at new mass scales. Furthermore, detailed dark matter simulations provide a theoretical ΛCDM baseline to link subhalo properties with observable galaxy characteristics. The conditional luminosity function, which describes the number of galaxies of luminosity $L \pm \mathrm{d}L/2$ in hosts of a given mass, can be combined with simulated subhalo populations in order to associate subhalo properties with observable characteristics (van den Bosch, Yang & Mo 2003; Yang, Mo & van den Bosch 2003; see further Vale & Ostriker 2004). This allows one to investigate the impact of baryonic physics on the galaxy distribution.

Our simulation set is more sensitive to possible dependence of the subhalo population on the host halo mass or redshift than previous works. Consequently, we can improve constraints on whether substructure properties are a function of M/M_*, where M_* is the characteristic mass of collapsing haloes defined by the scale at which the rms linear density fluctuation equals the threshold for non-linear collapse. One might expect that because low-mass haloes were mostly assembled much earlier when the universe was more dense, are at smaller M/M_* and lie where the power spectrum of mass fluctuations is steeper, that they might have significantly different subhalo distributions than more massive haloes. If subhaloes within low-mass and low-redshift haloes have a higher characteristic density (see e.g. Reed et al. 2005 and references therein), then they should be less subject to tidal stripping and disruption. Additionally, if the infall rate on to the host halo (i.e. merger rate) is different from the rate of subhalo destruction, then subhalo numbers will evolve with redshift.

The angular momentum of a cosmic (sub)halo is crucial to determine the radial distribution of its eventual stellar component (e.g. Mo, Mao & White 1998; van den Bosch et al. 2002; Verde et al. 2002) and its collapse factor compared with the parent dark matter halo (Stoehr et al. 2002). If high angular momentum material is systematically stripped from subhaloes, this would further inhibit the formation of stellar discs in dense environments consistent with observations (e.g. Goto et al. 2003). Also, a high collapse factor of the baryonic component would make the velocity dispersions of the stars eventually formed lower than that associated with the parent halo. This would exacerbate the apparent difference between the observed abundance of galaxy satellites and the predicted abundance of their host haloes, as discussed in detail in Stoehr et al. (2002) and Kazantzidis et al. (2004).

The angular momentum of the dark matter component of a subhalo will be relevant to its stellar properties only if star formation continues after infall and tidal stripping, which requires that sufficient baryons remain in the subhalo. While one generally expects much of the gas of a subhalo to be stripped upon infall, some of that gas may also be able to cool and form stars. Complex processes such as starbursts after infall and redistribution of baryonic angular momentum under tidal influences may affect the final spin of the baryonic component. Simulations predict starbursts will occur in gas-rich satellites as they are tidally stirred by the central potential (e.g. Mayer et al. 2001), which may explain the continuing star formation in Galactic satellites. However, a better understanding of post-infall star formation is needed to determine whether the angular momentum of the stellar component is correlated with that of the dark matter component.

Subhaloes are particularly sensitive to resolution issues (e.g. Moore, Katz & Lake 1996). Dark matter haloes and, by extension, subhaloes have densities that continually increase towards the halo centre, and so should be very difficult to disrupt completely unless numerical discreteness effects artificially lower the central density. A subhalo with a numerically softened cusp is more easily disrupted by the global tidal forces and interactions with other subhaloes that strip away the outer regions. Poor spatial resolution and two-body relaxation lower central densities, and so may lead to subhalo destruction, especially near host halo centres. Simulated clusters may generally suffer more from resolution issues than galaxies because of their later formation epoch, which means that cluster particles will have spent more time in low-mass haloes (Diemand et al. 2004a). Also, subhaloes with highly eccentric orbits are more likely to be disrupted because they pass near to the central potential.

In this work, we present the results of substructure analyses of 16 ΛCDM simulated haloes covering three decades in mass, from dwarfs to clusters, each with roughly a million particles. Our sample includes 10 clusters extracted from one cosmological volume (CUBEHI) to study cosmological variance, and also includes a seven million particle group and a four million particle cluster. Some of our haloes are well resolved to redshifts of three or higher, allowing investigation of mass or redshift-dependent trends. Additionally, we have modelled a cluster in power-law cosmologies where $P \propto k^n$ to analyse the dependence of the subhalo distribution on the spectral index, n.

2 NUMERICAL TECHNIQUES

2.1 The simulations

We use the parallel K–D (balanced binary) Tree (Bentley 1975) gravity solver PKDGRAV (Stadel 2001; see also Wadsley, Stadel & Quinn 2004) to model 16 dark matter haloes, further described in Reed et al. (2005); see Table 1. The CUBEHI run consists of a cube of 432^3 particles of uniform resolution. The six renormalized volume runs (e.g. Katz & White 1993; Ghigna et al. 1998) consist of a single halo in a high-resolution region nested within a lower resolution cosmological volume. Initial conditions for these high-resolution halo runs are created by first simulating a low-resolution cosmological volume. Next, a halo of interest is identified. To minimize sampling bias, volume-renormalized haloes are selected by mass with the only additional constraint that they do not lie within close proximity (2–3 $r_{\rm vir}$) to a halo of similar or larger mass. Then, the initial conditions routine is run again to add small-scale power to a region made up of high-resolution particles that end up within approximately two virial radii of the halo centre, while preserving the original large-scale random waves. This process is iterated in mass resolution increments of a factor of 8 until

Table 1. Summary of our halo sample at redshift zero. For volume-renormalized runs, the mass (h^{-1} $M_{\odot}$) and particle number of the central halo are listed. $v_{\rm cmax,host}$ is the host peak circular velocity (km s^{-1}). $N_{\rm p,eff}$ is the effective particle number based on the high-resolution region for renormalized runs. $v_{\rm c,lim}$ is the subhalo peak circular velocity (km s^{-1}) above which numerical disruption is insignificant.

	$M_{\rm halo}$	$v_{\rm cmax,host}$	$N_{\rm p,halo}$	$N_{\rm p,eff}$	$v_{\rm c,lim}$	$r_{\rm soft}$ (h^{-1} kpc)	$z_{\rm start}$	$L_{\rm box}$ (h^{-1} Mpc)	
CUBEHI	$0.7–2.1 \times 10^{14}$	710–1010	$0.6–1.6 \times 10^{6}$	432^3	50	5	69	50	10 clusters
GRP1	4×10^{13}	560	7.2×10^{6}	1728^3	40	0.625	119	70	Fornax mass
CL1	2.1×10^{14}	1020	4.6×10^{6}	864^3	60	1.25	119	70	Cluster
GAL1	2×10^{12}	244	0.88×10^{6}	2304^3	20	0.469	119	70	Milky Way
GRP2	1.69×10^{13}	460	0.38×10^{6}	864^3	60	1.25	119	70	Group
DWF1	1.88×10^{11}	130	0.64×10^{6}	4608^3	15	0.234	119	70	Two dwarfs
	1.93×10^{11}	130	0.66×10^{6}						
$n = 0$	1.9×10^{14}	1300	0.54×10^{6}	432^3		2.5	799	70	$P \propto k^{0}$
$n = -1$	2×10^{14}	1110	0.55×10^{6}	432^3		2.5	269	70	$P \propto k^{-1}$
$n = -2$	1.6×10^{14}	870	0.45×10^{6}	432^3		2.5	99	70	$P \propto k^{-2}$
$n = -2.7$	2.9×10^{13}	470	0.82×10^{5}	432^3		2.5	79	70	$P \propto k^{-2.7}$

the desired resolution is achieved. We have verified that the high-resolution haloes are free from significant contamination by massive particles.

Our largest halo has seven million particles and most have $\sim 10^6$ particles within the virial radius at redshift zero. As a result of the high sensitivity of the subhalo distribution to numerical resolution effects, we only consider haloes with at least 3.5×10^5 particles. We adopt a ΛCDM cosmology with $\Omega_{\rm m} = 0.3$ and $\Lambda = 0.7$. The initial density power spectrum is normalized such that σ_8 extrapolated to redshift zero is 1.0, consistent with both the cluster abundance (see e.g. Eke, Cole & Frenk 1996 and references therein) and the *WMAP* normalization (e.g. Bennett et al. 2003; Spergel et al. 2003). We use a Hubble constant of $h = 0.7$, in units of 100 km s^{-1} Mpc^{-1}, and assume no tilt (i.e. a primordial spectral index of 1). To set the initial conditions, we use the Bardeen et al. (1986) transfer function with $\Gamma = \Omega_{\rm m} \times h$. For the volume-renormalized runs, we list the effective particle number of the highest resolution region rather than the actual particle number in Table 1. Numerical parameters are consistent with empirical studies (e.g. Moore et al. 1998; Stadel 2001; Power et al. 2003; Reed et al. 2003).

2.2 The analysis

The host haloes are defined using the spherical overdensity (SO) algorithm (Lacey & Cole 1994) with a top hat overdensity based on Eke et al. (1996) where the ΛCDM virial overdensity, $\Delta_{\rm vir}$, in units of critical density is approximately 100. Bound subhaloes are identified using SKID (Stadel 2001; http://www-hpcc.astro.washington.edu/tools/skid.html), which uses local density maxima to identify bound mass concentrations independently of environment. SKID iteratively slides particles towards higher densities until a converged group of particles is found. The radial extent of each SKID halo is determined by the distribution of bound particles and no predetermined subhalo shape is imposed. The maximum circular velocity of each subhalo, $v_{\rm c,max}$, is calculated from the measured peak of the rotation curve $v_{\rm c}(r) = [GM(<r)/r]^{0.5}$. For virialized host haloes, the ratio of $v_{\rm cmax,host}/v_{\rm c,host}(r_{\rm vir})$ depends primarily on M/M_* and is readily estimated from the halo density profile given in Reed et al. (2003b). Typical values of $v_{\rm cmax,host}/v_{\rm c,host}(r_{\rm vir})$ are 1.5–1.6 for our dwarfs and 1.05–1.25 for our clusters at redshift zero, declining to smaller values at higher redshift for each halo. To test for self-similarity between haloes, we thus normalize the velocity distribution function (VDF) to the peak circular velocities of hosts. We note that a subhalo bound to another subhalo will sometimes be catalogued as a separate SKID subhalo, particularly when the chosen linking parameter τ is small. Our tests indicate that the VDF is insensitive to τ except for the few largest subhaloes. We set $\tau = 2r_{\rm soft}$ for the CUBEHI run and $\tau = 4r_{\rm soft}$ for all other simulations. We consider only subhaloes of 32 or more particles in our analyses, consistent with Ghigna et al. (1998) and Springel et al. (2001). For analyses of subhalo angular momenta, we adopt an empirically motivated minimum of 144 particles per subhalo; see Section 3.2. Differential plots of binned quantities use the median value of each bin and bin sizes are variable in increments of $\Delta\log_{10} = 0.1$, but increased when necessary so that no bins are empty.

2.3 A resolution study and the radial distribution of subhaloes

For our volume-renormalized runs, GAL1, GRP1 and CL1, we have analysed 3, 2 and 1 identical lower resolution versions, respectively, where the mass resolution is varied by increments of a factor of 8. To find the minimum subhalo circular velocity down to which our results are complete, $v_{\rm c,lim}$, we plot the subhalo circular VDF for each simulation and identify the $v_{\rm cmax}$ below which the VDF slope begins to flatten as a result of incompleteness, as described in Ghigna et al. (2000). In Fig. 1, we plot the resolution criteria for halo GRP1, marking our conservative $v_{\rm c,lim}$ completeness limits. The agreement of the lower resolution versions shows that this technique is sound. Less conservative (but still apparently sound) completeness limits for our halo sample would have yielded roughly $v_{\rm c,lim} \propto N_{\rm p,halo}^{1/3}$ for each of our three haloes with multiple resolutions. Numerical effects on the subhalo population are likely manifested more strongly for low-redshift subhaloes, because they have been subject to potentially disrupting events for more time. This implies that measuring $v_{\rm cmax}$ at $z = 0$ should still be valid at a higher redshift. We have verified that the $z = 0$ $v_{\rm c,lim}$ for halo GRP1 remains valid at $z = 1$ where the highest resolution version still has 3.5×10^6 particles. Additionally, we have considered whether the completeness limits, which were obtained using subhaloes within the entire virial volume, may change at small radii, where numerical problems are expected to be stronger. We find that even when the sample is limited to $r < 0.3r_{\rm vir}$, the $v_{\rm c,lim}$ derived from the entire virial volume as described above, remains valid.

The radial distribution of the subhalo population, shown for GRP1 in Fig. 2, has a slope equal to or shallower than the slope of the density profile for each resolution at all radii. At very small radii,

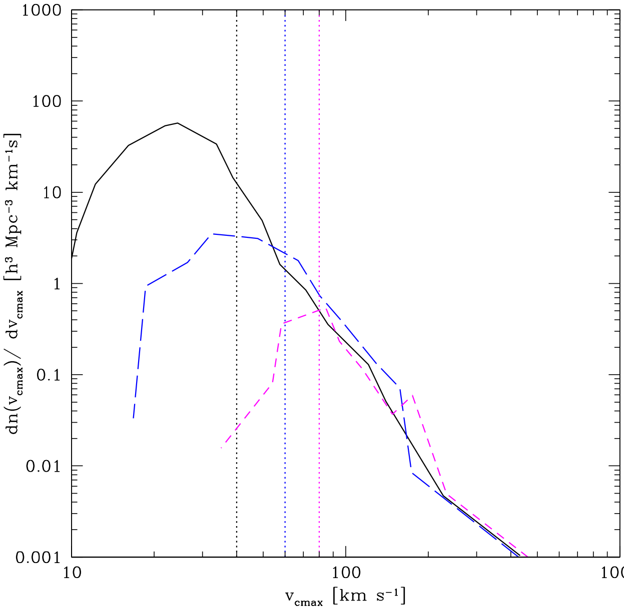

Figure 1. Velocity distribution function (VDF) for halo GRP1 (at $z = 0$) with seven million particles and for two lower resolutions, with particle mass incrementally increasing by a factor of 8. The circular velocity completeness limit $v_{c,lim}$ is marked for each resolution with a vertical line.

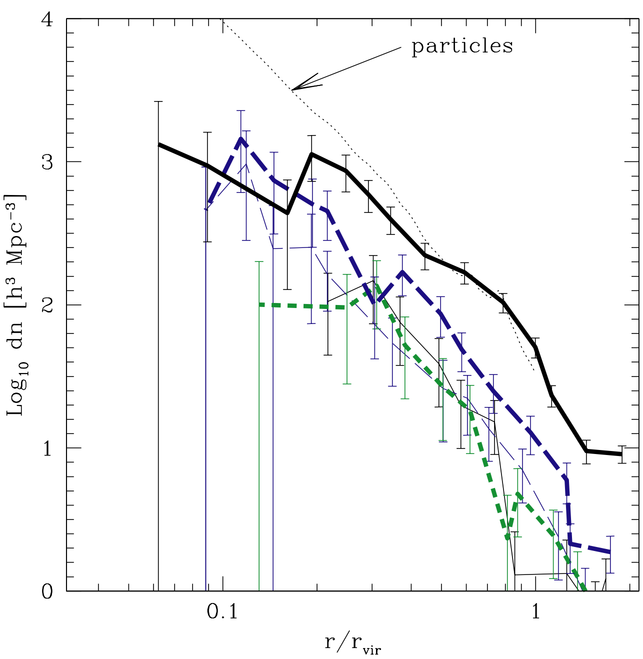

Figure 2. The $z = 0$ radial distribution of subhaloes in GRP1 for each of the three different resolutions (solid, long-dashed and short-dashed are the highest, middle and lowest resolution runs, respectively). Thin lines have the $v_{c,lim}$ resolution limit of the lowest resolution run applied. 1σ Poisson error bars are shown. The dotted line is the particle distribution with arbitrary normalization.

subhaloes are highly deficient, possibly as a result, at least in part, of artificial disruption by the tidal forces from the central mass concentration. When a subhalo migrates inwards via dynamical friction to a radius where its central density is lower than the local density of the host halo, it will likely be disrupted (e.g. Syer & White 1998). Numerical disruption enhanced by the strong tides near host centres could affect subhaloes. The flattened slope of the radial subhalo distribution of GRP1 subhaloes relative to the mass profile interior to roughly $0.2r_{\rm vir}$ for our highest resolution and interior to $0.3r_{\rm vir}$ for our lowest resolution implies that disruption and/or stripping of subhaloes is important in the halo central region. The increase in radius of the break in subhalo slope with decreasing resolution suggests that numerical disruption, if present, is worse for lower resolutions. However, we caution that the location of the break is not well defined because of Poisson uncertainties. Given the uncertainties, it is not possible to reliably separate spurious from real disruption that may be present in our simulations at small radii. Thus, we have no evidence that the central substructure number density has converged with resolution. Increasing the mass resolution by a factor of 8 results in roughly a factor of ∼2–2.5 more subhaloes at a given radius beyond roughly $0.3r_{\rm vir}$, though there is substantial noise in this estimate. At larger radii, where numerical effects are less important, a subhalo radial distribution that is shallower than the mass profile is favoured in our data, and is also reported by De Lucia et al. (2004), Stoehr et al. (2003), Diemand et al. (2004), Gao et al. (2004a,b), Gill, Knebe & Gibson (2004a) and Nagai & Kravtsov (2005). However, a radial subhalo slope equal to the mass profile slope is not ruled out except in the central region where numerical effects may dominate. Note that if we use only a minimum mass cut without imposing the circular velocity completeness limit, a more significant antibias in the radial distribution is found (see also Nagai & Kravtsov 2005).

3 RESULTS

3.1 The circular velocity distribution function (VDF)

In Fig. 3, we plot the cumulative VDF for all haloes at redshift zero. Our completeness and resolution limits exclude the majority

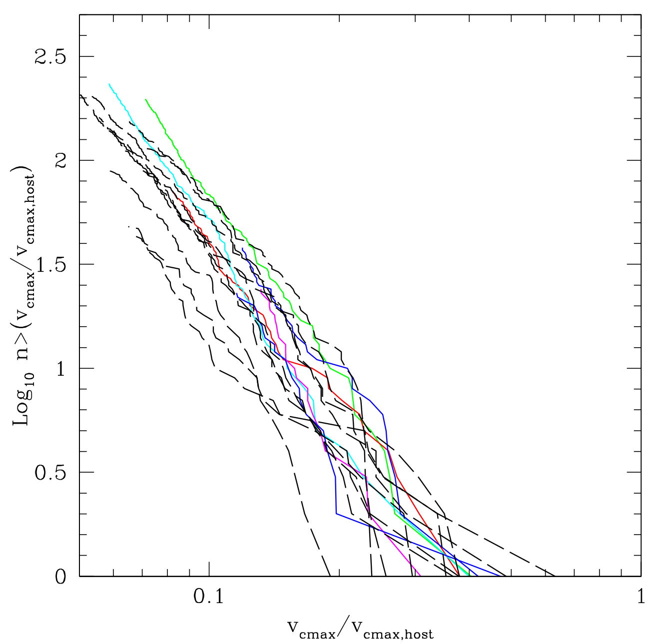

Figure 3. The $z = 0$ cumulative subhalo velocity distribution function (VDF) with the completeness limits $v_{c,\rm lim}$ applied and considering only subhaloes with 32 or more particles, plotted as a function of $v_{\rm cmax}/v_{\rm cmax,host}$. Solid lines are renormalized volumes (green, light blue, magenta, red and blue for CL1, GRP1, GRP2, GAL1 and DWF1, respectively). Dashed lines (black) are the 10 clusters in the CUBEHI simulation.

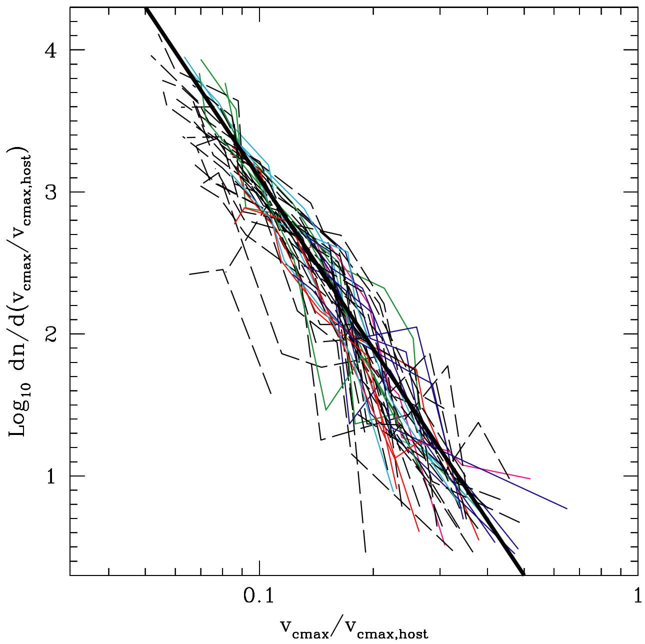

Figure 4. Normalized subhalo velocity distribution function (VDF) for all haloes with $N_p > 3.5 \times 10^5$ at redshifts 0, 0.5, 1 and 2, normalized to $v_{\rm cmax,host}$ and a virial volume of unity. Solid lines (colours as in Fig. 3) are renormalized volumes, dashed lines (black) are the 10 clusters in the CUBEHI simulation. Heavy solid line corresponds to $\mathrm{d}n/\mathrm{d}v = \frac{1}{8}(v_{\rm cmax}/v_{\rm cmax,host})^{-4}$.

of subhaloes identified by SKID, leaving of the order of 100 subhaloes in most hosts. Fig. 4 shows the differential VDF for our entire set of subhaloes at $0 \leqslant z \leqslant 2$ for hosts of more than 3.5×10^5 particles. The subhalo VDF is well approximated by a power law with slope and normalization given by

$$\mathrm{d}n/\mathrm{d}v = \frac{1}{8}\left(\frac{v_{\rm cmax}}{v_{\rm cmax,host}}\right)^{-4}, \tag{1}$$

over the range of approximately $0.07v_{\rm cmax,host}$ to $0.4v_{\rm cmax,host}$ with halo to halo scatter of a factor of roughly 2 to 4. When we individually consider the VDF for hosts of different mass, we find no evidence of mass dependence on the VDF amplitude or slope in our data and similarly we detect evidence of weak or zero redshift dependence (see below). This implies that the number density of subhaloes is approximately self-similar, independent of the mass and redshift of the host halo. Here, we caution that a larger halo sample would be needed to identify any weak trends (e.g. an increase in substructure abundance with halo mass, reported by Gao et al. 2004a) as they would be masked by the large halo to halo scatter. The farthest low VDF outlier halo is the largest cluster in the CUBEHI simulation at $z = 1$, which has approximately 4.5×10^5 particles at the time. In Fig. 5, we present the VDF of our highest resolution halo to redshift $z \simeq 4$. There is little or no evolution in VDF slope or normalization, although there are fewer large subhaloes at high redshift, as seen by the lack of data points in the VDF beyond large $v_{\rm cmax}/v_{\rm cmax,host}$ in high-redshift hosts. Thus, large subaloes are deficient until lower redshifts when they either infall on to the host or are formed as merger products of existing subhaloes.

In Fig. 6, we present the non-normalized differential VDF for our entire set of subhaloes, which displays little or no redshift evolution

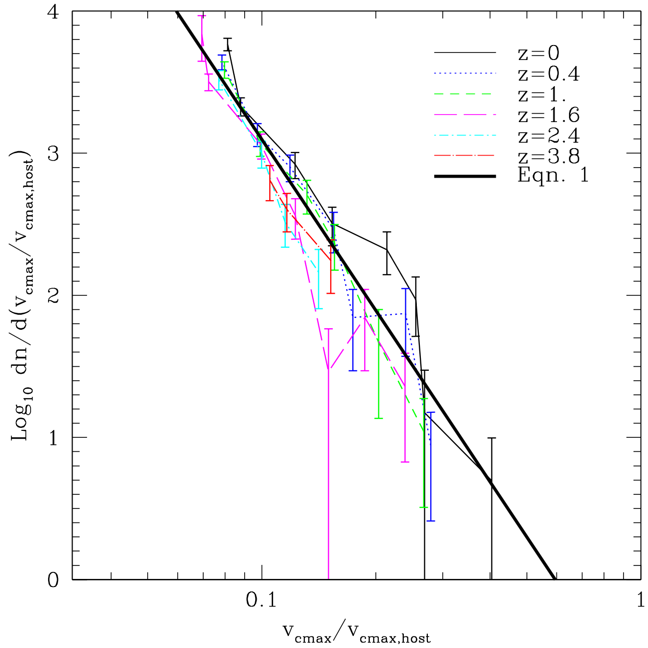

Figure 5. Evolution of the normalized subhalo velocity distribution function (VDF) for halo GRP1. Subhalo circular velocities are normalized to $v_{\rm cmax,host}$ and a virial volume of unity.

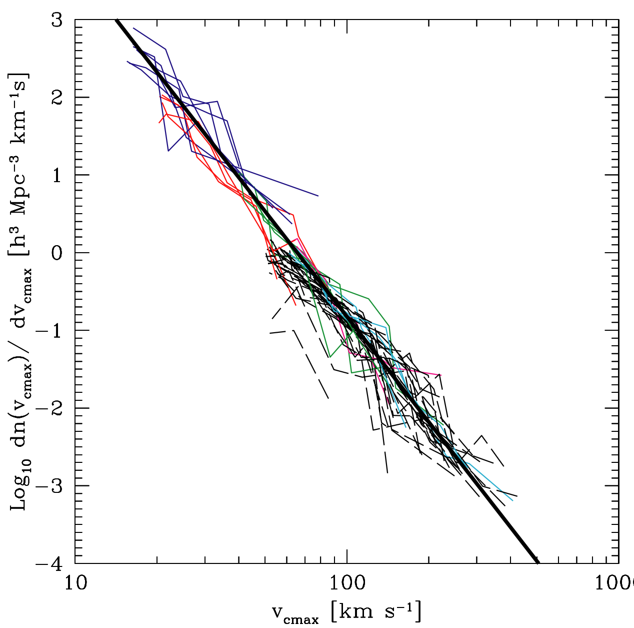

Figure 6. Differential subhalo velocity distribution function (VDF) for all haloes with $N_p > 3.5 \times 10^5$ at redshifts 0, 0.5, 1 and 2. Solid lines (colours as in Fig. 3) are renormalized volumes, dashed lines (black) are the 10 clusters in the CUBEHI simulation. The heavy solid line denotes $\mathrm{d}n/\mathrm{d}v = 0.5 \times 10^8 v_{\rm cmax}^{-4.5}$ (equation 2). Volume units are comoving.

in comoving space. The subhalo VDF is fit by

$$\mathrm{d}n/\mathrm{d}v = 1.5 \times 10^8 v_{\rm cmax}^{-4.5}\,(h^3\,\mathrm{Mpc^{-3}\,km^{-1}\,s}), \tag{2}$$

for subhaloes of 20–300 km s^{-1} in hosts of 10^{11} to 10^{14} M$_\odot$ and redshifts from zero to two, with scatter of a factor of ~2–4. This slope of this non-normalized VDF is steeper because lower mass galaxies

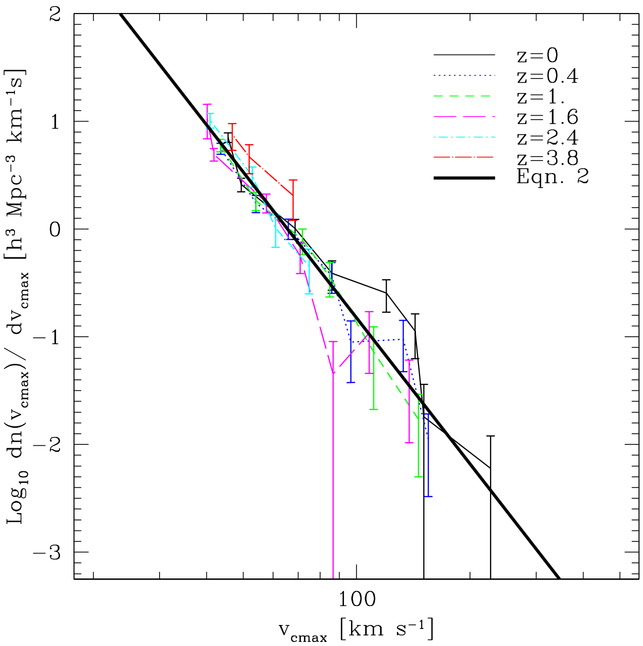

Figure 7. Subhalo velocity distribution function (VDF) in comoving coordinates for the group GRP1, which still has over half a million particles at $z = 3.8$. 1σ Poisson error bars are shown.

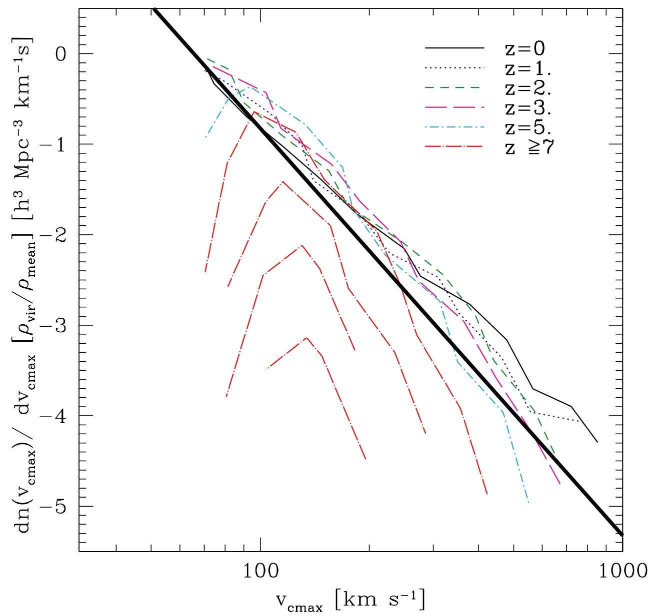

Figure 8. Velocity distribution function (VDF) for friends-of-friends (FOF) haloes in the CUBEHI simulation plotted for $0 \leqslant z \leqslant 15$. Heavy solid line is the fit to the subhalo population given by equation (2) (non-normalized). For reference, we normalize the FOF VDF to the virial overdensity as a function of redshift by multiplying by a factor of $\rho_{\mathrm{virial}}/\bar{\rho}$.

in the sample have a larger ratio of $v_{\mathrm{cmax,host}}/v_{\mathrm{c,host}}(r_{\mathrm{vir}})$. The dependence on $v_{\mathrm{cmax,host}}/v_{\mathrm{c,host}}(r_{\mathrm{vir}})$ implies that this non-normalized VDF is unlikely to hold universally. Fig. 7 shows that the non-normalized subhalo VDF for GRP1 has weak or no evolution to $z \simeq 4$.

We also calculate the VDF of friends-of-friends (FOF; Press & Davis 1982; Davis et al. 1985) haloes, from which the population of subhaloes must have descended. The FOF algorithm identifies virialized haloes that are not part of larger virialized objects. In Fig. 8, we plot the VDF for all FOF haloes in the CUBEHI simulation adopting a linking length of 0.2 times the mean particle separation. We have normalized the FOF VDF by multiplying it by the mean virial overdensity, $\rho_{\mathrm{virial}}/\bar{\rho}$, at each redshift. Differences between the subhalo and halo VDFs are generally smaller than a factor of 3 until $z \gtrsim 7$, in agreement with $z = 0$ results by Gao et al. (2004a). At $z \gtrsim 5$, the FOF VDF drops rapidly with increasing redshift, presumably as a result of the fact that it samples the steep drop-off regime of the mass function at high redshift. Higher redshift simulations are needed to test whether the lower FOF VDF at $z \gtrsim 7$ results in small subhalo numbers for extremely high-redshift hosts.

3.2 Subhalo angular momenta

We analyse the subhalo angular momenta given by the spin parameter, $\lambda = LE^{1/2}/GM^{1/2}$ (Peebles 1969), for subhaloes at redshift zero in our two highest resolution simulations, GRP1 and CL1. Angular momentum L is calculated with respect to the centre of mass of the subhalo. Energy $E = E_{\mathrm{kinetic}} + E_{\mathrm{potential}}$ is summed over all subhalo particles. Each central subhalo and subhaloes with more than 50 000 particles (for computational speed) are excluded. In our simulations, median subhalo λ increases with decreasing particle number once below ~100 particles, indicating an upward bias for poorly resolved haloes. We thus limit our spin analyses to subhaloes containing 144 or more particles, which results in no dependence of median spin on subhalo mass. Several studies have found the lognormal function to be a good description of halo spins

$$p(\lambda)\,\mathrm{d}\lambda = \frac{1}{\sigma_\lambda\sqrt{2\pi}}\exp\left[-\frac{\ln^2(\lambda/\lambda_0)}{2\sigma_\lambda^2}\right]\frac{\mathrm{d}\lambda}{\lambda} \tag{3}$$

(Barnes & Efstathiou 1987; Ryden 1988; Warren et al. 1992; Cole & Lacey 1996; Gardner 2001; van den Bosch et al. 2002; Vitvitska et al. 2002; Aubert, Pichon & Colombi 2004; Colin et al. 2004; Peirani, Mohayaee & Pacheco 2004), where λ_0 and σ_λ are fit parameters. Fig. 9 compares the histogram of subhalo spins with the best-fitting χ^2 lognormal function given by $(\lambda_0, \sigma_\lambda) = (0.0235, 0.54)$ and $(0.0238, 0.73)$ for halo GRP1 and CL1, respectively. Median and arithmetic average values of $\lambda_{\mathrm{med}} = 0.024$ and $\lambda_{\mathrm{avg}} = 0.027$ for GRP1 subhaloes, and $\lambda_{\mathrm{med}} = 0.024$ and $\lambda_{\mathrm{avg}} = 0.026$ for CL1 subhaloes. Subhalo spins are significantly smaller than spins of a sample containing 1.5×10^4 field haloes selected from the CUBEHI volume using the SO algorithm, which has $\lambda_{\mathrm{med}} = 0.037$ and $(\lambda_0, \sigma_\lambda) = (0.037, 0.57)$ over the mass range of 1.9×10^{10}–6.5×10^{12} (144–50000) particles. Within this field halo sample and within the subhalo samples, spins have no significant mass dependence, so comparisons between differing mass scales of different simulations should be valid. Our field angular momenta are consistent with a number of recent studies that find $\lambda_0 = 0.035$–0.046 for virialized ΛCDM haloes (Bullock et al. 2001; van den Bosch et al. 2002; Vitvitska et al. 2002; Aubert et al. 2004; Colin et al. 2004; Peirani et al. 2004). Note that some of these studies use a slightly different definition of spin introduced by Bullock et al. (2001) that has some dependence on the density profile.

Given that our subhaloes are in high-density environments, it is likely that their spins are lowered by the removal of high angular momentum material, which should be most vulnerable to tidal stripping. We verify that stripping of outer material has the potential to lower spins by the required amounts by measuring spins for the central regions of SO haloes in the CUBEHI volume. Here, we find that the central SO region containing 15 times the usual virial

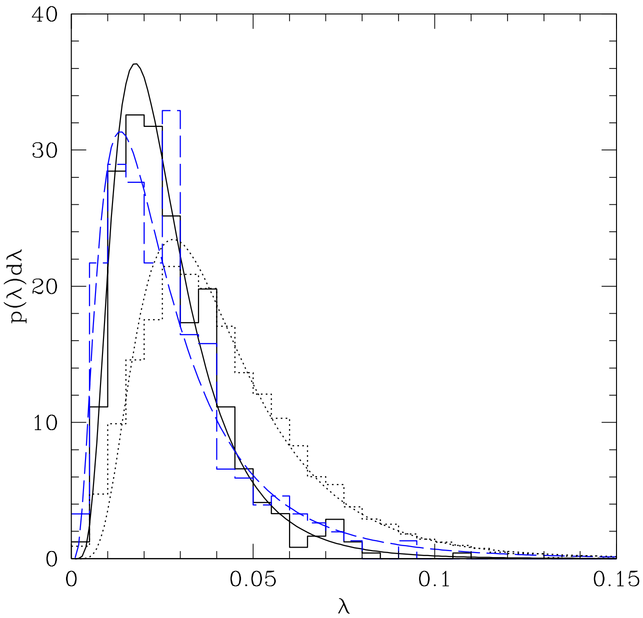

Figure 9. Histograms show the $z = 0$ distribution of spin subhalo parameters within halo GRP1 (solid) and halo CL1 (dashed) for subhaloes with 144 or more particles. Spins of spherical overdensity (SO) field haloes from the CUBEHI volume are shown by dotted lines. Curves are fits to the lognormal distribution described in text.

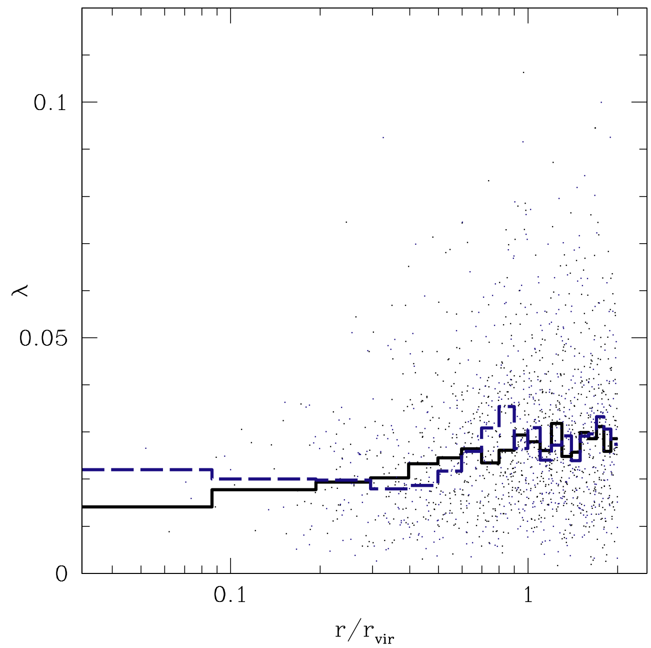

Figure 10. Radial dependence of spin parameter at $z = 0$. Solid (dashed) histogram is median of subhalo spins for host GRP1 (CL1).

overdensity has $\lambda_{\rm med} = 0.025$, which is similar to $\lambda_{\rm med}$ for subhaloes. This overdensity generally contains the central ∼15–30 per cent of the SO mass. We have also determined that the SO haloes whose central materials have the lowest spins relative to the surrounding halo material are the high-spin SO haloes that comprise the tail of the lognormal distribution. This suggests that subhaloes with initially high spins are likely to be the largest contributors to the removal of subhalo angular momentum. Interestingly, the central regions of low-spin SO haloes ($\lambda \ll \lambda_{\rm med}$) generally have higher spin than the surrounding halo material.

An alternative explanation for the low spins of subhaloes may be related to the fact that (sub)halo mass growth is generally halted upon infall into a larger halo. For the case of field haloes, spins decrease over time in the absence of major mergers, particularly in the period immediately following a major merger event (e.g. Vitvitska et al. 2002; Peirani et al. 2004). If a similar decrease in spin occurs in the high-density environments within haloes, then it could contribute to the low subhalo spins. More study is needed to determine whether this mechanism for lowering spin is effective for subhaloes.

The radial dependence of subhalo spins shown in Fig. 10 shows that local environment directly affects subhalo spin. Median subhalo spin decreases with decreasing radius from $\lambda \simeq 0.025$–0.03 near $r_{\rm vir}$ to $\lambda \simeq 0.02$ at $0.3r_{\rm vir}$, where tidal effects are greater. The transition in spins from subhaloes to field haloes at $r_{\rm vir}$ is smooth, and spins of SKID haloes found between $r_{\rm vir}$ and $2r_{\rm vir}$ have weak or no further radial dependence. Note that the median SKID halo spin $\lambda_{\rm med} \simeq 0.03$ between $r_{\rm vir}$ and $2r_{\rm vir}$ is somewhat smaller than for SO haloes selected from the uniform volume. We have tested that when the field SO haloes of the large volume (CUBEHI) are instead selected with SKID, their spins are smaller than with SO, but only by 5–10 per cent, which is not enough to explain the small spins found in the high-density regions. This suggests that field haloes in the high-density environments just outside of larger virialized haloes have spins that are ∼10 per cent lower than for the global population. Spins in high-density regions could be reduced as a result of a contribution from subhaloes whose orbits have previously taken them within the virial radius (Gill, Knebe & Gibson 2005), causing stripping of high angular momentum material. Additionally, tidal interactions with the massive neighbouring halo (Gnedin 2003; Kravtsov, Gnedin & Klypin 2004b) may also have some impact on spin. This relatively weak environmental dependence on field halo spins is still consistent with Lemson & Kauffmann (1999), who found no difference in spins of virialized haloes in mild over(under)densities.

The radial trend in spins could be observable if reliable spins can be estimated for a large sample of cluster galaxies or satellites in external systems and if spin of baryonic material can be used as a tracer of subhalo spin. Galaxies that form from low-spin material should have larger collapse factors. If star formation occurs after subhalo angular momentum has been lowered, then galaxies nearer to host centres may thus have smaller radial extent than galaxies near or outside the virial radius, although complex baryonic processes related to star formation may dominate over any potential spin-induced trend in stellar distribution (see Stoehr et al. 2002; Hayashi et al. 2003; Kazantzidis et al. 2004). The central galaxy would likely deviate from this trend because it undergoes late mergers, which have been shown to increase halo angular momentum (Gardner 2001; Vitvitska et al. 2002).

A radial trend in subhalo spins is unlikely to be easily observable unless the stellar component of a galaxy is assembled subsequent to infall and stripping of high-spin material. If gas infall, star formation and disc growth all cease soon after infall, then spins of galaxies hosted by subhaloes would only reflect the spin of the original dark matter halo. If however, sufficient gas remains after accretion into another dark matter halo that there is some continuing star formation (as for Galactic satellites), then the stellar and gaseous distribution may have a smaller spin than that of the dark matter host prior to infall. Numerical simulations are needed to determine the extent that subhalo baryonic spins reflect the spins of their host dark matter subhaloes.

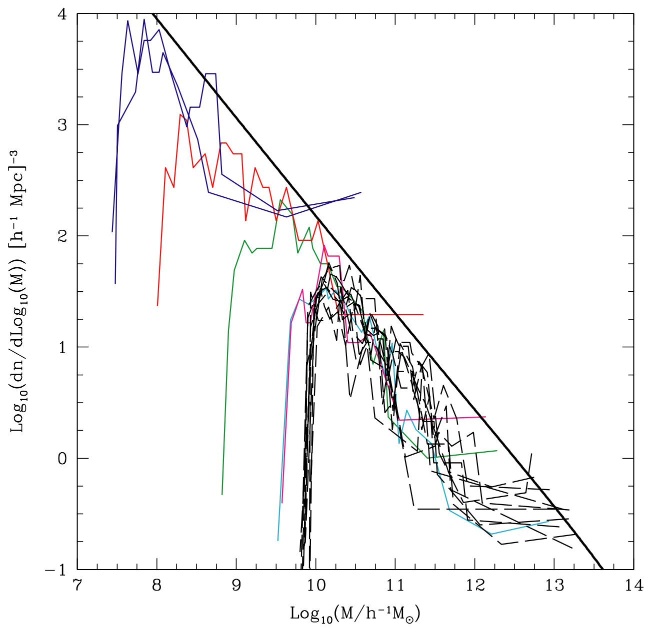

Figure 11. The mass function of the subhalo population for each of our haloes at $z = 0$. Heavy dark line is the Sheth & Tormen (1999) prediction for virialized haloes, which closely matches the low redshift friends-of-friends (FOF) mass function, and is normalized by a simple factor equal to the virial overdensity ($\rho_{\rm virial}/\bar{\rho}$) for reference.

3.3 Subhalo mass function

We plot the subhalo mass function at $z = 0$ (Fig. 11) and at $z = 1$ (Fig. 12). The steep drop on the low-mass end for each halo is the result of exclusion of haloes with $v_{\rm cmax} < v_{\rm c,lim}$ for each simulation. The subhalo mass function is independent of halo mass, a result also seen in De Lucia et al. (2004), although a weak mass dependence such as that reported by Gao et al. (2004a) is not ruled out by our data. The Sheth & Tormen (1999) function normalized by a factor equal to the virial overdensity is plotted for reference. The Sheth and Tormen function, a modification of the Press & Schechter (1974) formalism, is an excellent match to the CUBEHI FOF mass function at low redshifts (Reed et al. 2003). The factor of approximately 2 to 3 offset between the subhalo mass function and the FOF mass function is independent of mass and redshift, which implies that the stripping efficiency of subhaloes is largely mass and redshift independent, though infall timing and evolution of the global mass function may also affect the subhalo mass function.

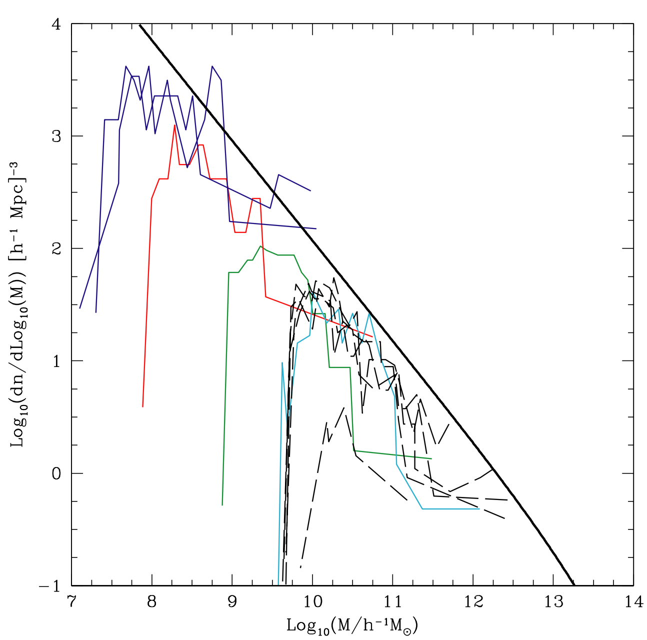

Figure 12. Subhalo mass function, as in Fig. 11, except at $z = 1$.

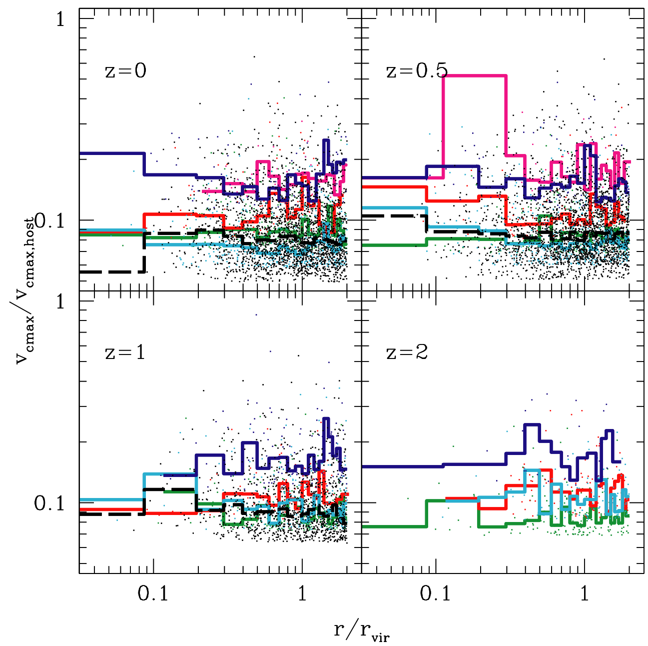

Figure 13. The $v_{\rm cmax}/v_{\rm cmax,host}$ distribution of subhaloes plotted against radial position at redshifts 0 (top left), 0.5 (top right), 1 (bottom left) and 2 (bottom right). Individual histograms represent the median $v_{\rm cmax}/v_{\rm cmax,host}$ from each simulation with colours as in Fig. 3 [e.g. dashed (black) histogram is an average of 10 CUBEHI clusters]. Coloured points are from the normalized runs with same colours as before and black points are from the CUBEHI run. The subhalo associated with the potential centre is excluded from each halo. Subhaloes from hosts with less than 3.5×10^5 particles are again excluded.

3.4 Radial distribution and subhalo orbits

In Fig. 13, we show the distribution of subhalo $v_{\rm cmax}$ versus radial position for a range of redshifts. There are no clear radial trends in $v_{\rm cmax}$ for $z \leqslant 2$. However, Fig. 14 shows that subhaloes near the centres of their hosts tend to have lower median masses than subhaloes at larger radii, a trend consistent with e.g. Taffoni et al. (2003; see also De Lucia et al. 2004; Gao et al. 2004a; Kravtsov et al. 2004b; Taylor & Babul 2004), indicative of tidal stripping near halo centres (e.g. Tormen, Diaferio & Syer 1998). This suggests that the morphology–radius relation seen in clusters (e.g. Whitmore & Gilmore 1991) cannot be explained by a $v_{\rm cmax}$–radius relation. We note that the region where the median mass is smallest (less than $\sim 0.3 r_{\rm vir}$ is also the least numerically robust, discussed in Section 2.3.

In Fig. 15, we show the circularity of subhalo orbits, $L/L_{\rm circ}$, which is the angular momentum that a subhalo with a given orbital energy would have if it were on a circular orbit. Orbits are calculated from a snapshot position and velocity of each substructure applied to a static spherical approximation of the host halo potential, which is computed from the mass profile as in Ghigna et al. (1998). Our

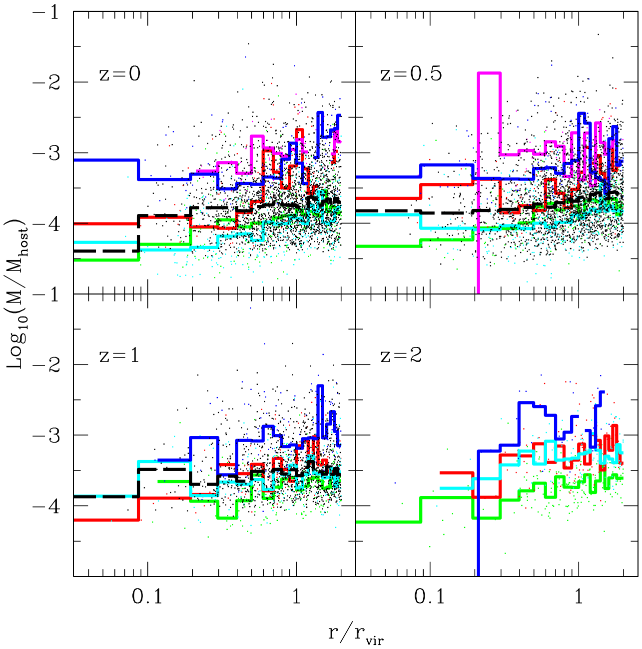

Figure 14. The M/M_{host} distribution of subhaloes plotted against radial position at redshifts 0 (top left), 0.5 (top right), 1 (bottom left) and 2 (bottom right). Individual histograms represent the median M/M_{host} from each simulation as in Fig. 13.

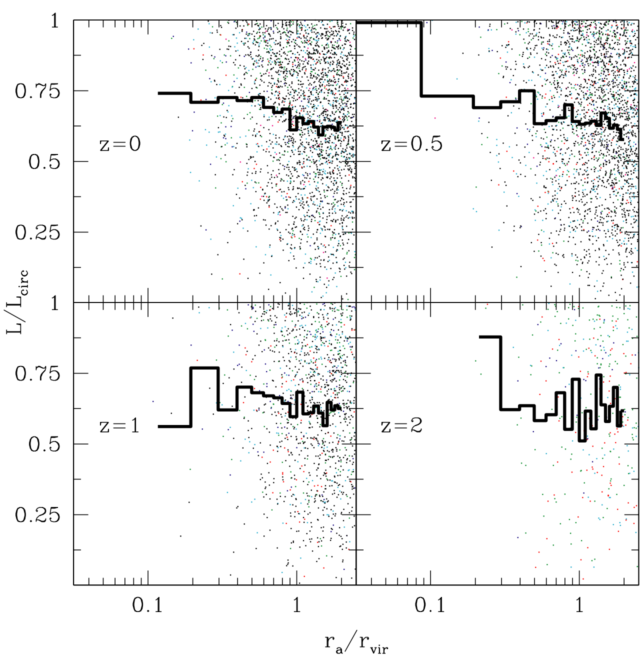

Figure 15. The circularity of subhalo orbits, L/L_{circ} versus $r_{\mathrm{a}}/r_{\mathrm{vir}}$, for the same haloes and redshifts as in Figs 13–14. L_{circ} is the orbital angular momentum of a subhalo on a circular orbit of a given orbital energy. r_{a} is the subhalo apocentre. Histogram represents the average L/L_{circ}.

subhaloes have mean circularities between 0.6 to 0.7 where sampling is high, with a redshift zero mean $L/L_{\mathrm{circ}} = 0.64$ for $r < r_{\mathrm{vir}}$. The subhalo circularity increases weakly at small radii for lower redshifts, suggesting circularisation of orbits over time as seen in simulations by Gill et al. (2004). Also, there are a larger number of subhaloes in the nearly circular orbits than in the most radial orbits, especially at low redshift. Both of these trends may be a

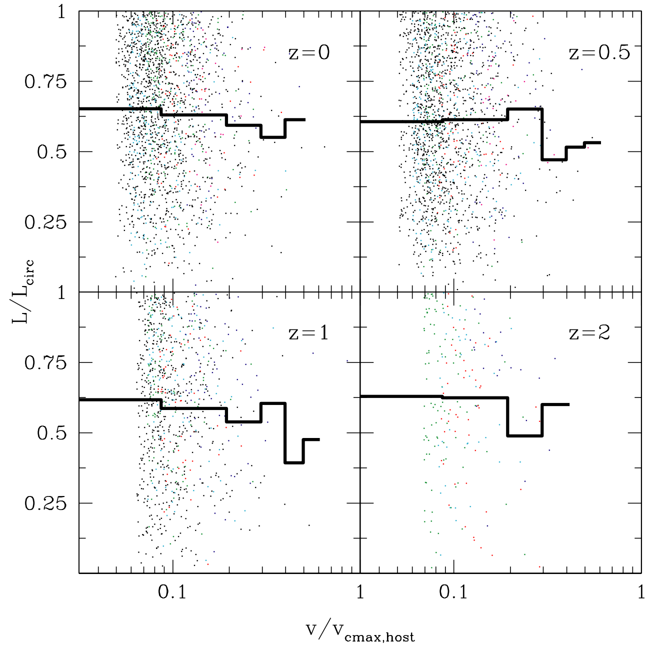

Figure 16. The circularity of subhalo orbits, L/L_{circ} versus ($v_{\mathrm{cmax}}/v_{\mathrm{cmax,host}}$), for the same redshifts as in Figs 13–15, here limited to subhaloes within r_{vir}. Average circularity given by histogram.

result of disruption or heavy stripping of subhaloes on extremely radial orbits because they pass nearer the cluster central potential. This effect would be greatest for subhaloes with small apocentres. In Fig. 16, we present the circularity as a function of $v_{\mathrm{cmax}}/v_{\mathrm{cmax,host}}$. Again, there are no strong trends, except that small subhaloes with very radial orbits appear to be relatively deficient, especially at low redshift.

Fig. 17 shows the three dimensional velocity dispersion of subhaloes, $\sigma_{3\mathrm{D}}$, as a function of radius at redshift zero. The velocity

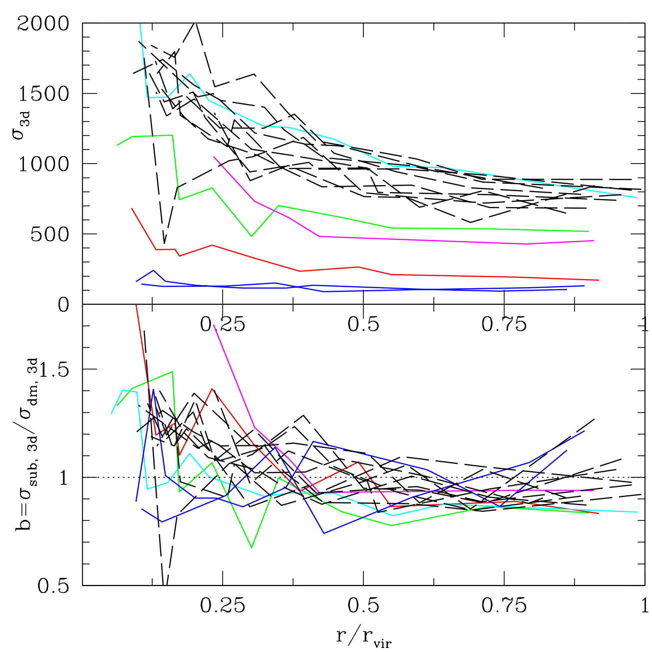

Figure 17. Top: $\sigma_{3\mathrm{D}}$ versus radius at $z = 0$ for each halo. Bottom: subhalo velocity bias, $b = \sigma_{\mathrm{sub,3D}}/\sigma_{3D,dm}$. Line types and colours are the same as Fig. 3.

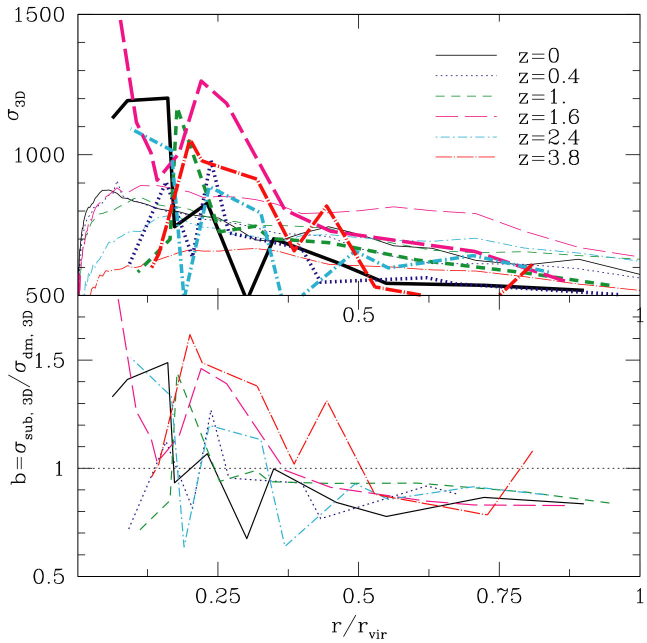

Figure 18. Top: evolution of velocity dispersions for the seven million particle group GRP1. Thick lines are σ_{3D} of the subhalo distribution. Thin lines are σ_{3D} for particle distribution. Bottom: subhalo velocity bias for the same redshifts.

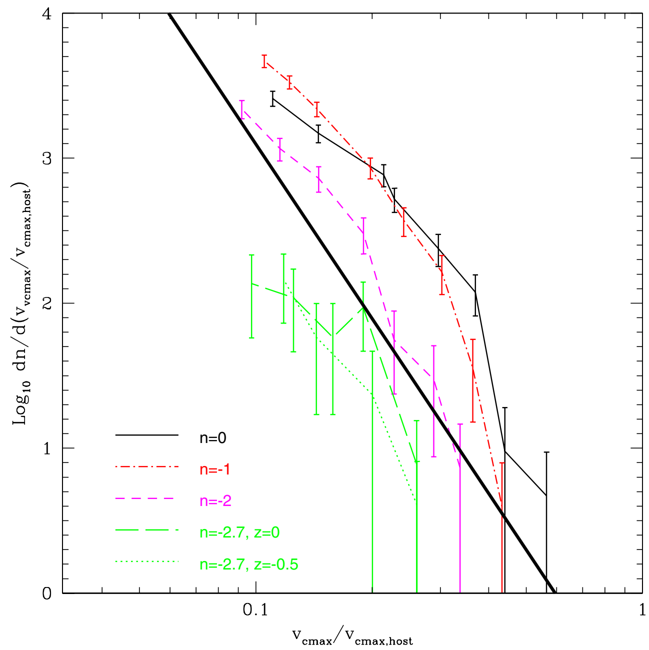

Figure 19. Subhalo velocity distribution function (VDF) for our cluster with initial power spectrum given by $P \propto k^n$. Heavy solid line is a fit to ΛCDM haloes.

dispersion is flat or slowly decreasing with radius at $\geqslant 0.5 r_{vir}$. At smaller radii, σ_{3D} generally increases moderately towards the centre, reaching less than 1.5–$2\sigma_{3D}(r_{vir})$. Subhalo orbital motions suggest a velocity bias $b = \sigma_{sub,3D}/\sigma_{3D,dm}$ (bottom panel of Fig. 17) that increases with decreasing radius, reaching ∼1.2 by $\sim 0.2 r_{vir}$, similar to that found in e.g. Colin, Klypin & Kravtsov (2000), Ghigna et al. (2000) and Diemand et al. (2004b). Diemand et al. attribute both their central velocity bias and their central spatial antibias to tidal destruction of slow moving subhaloes near the cluster centre. Note that in a dynamically relaxed system, a spatial antibias automatically results in a positive central velocity bias (see e.g. van den Bosch et al. 2004). At radii $\gtrsim 0.5 r_{vir}$, there is also a hint of a weak velocity antibias of ∼10 per cent in many haloes, although subhalo velocities are consistent with no large radius antibias when the range of halo to halo scatter and uncertainty resulting from small numbers of subhaloes is considered. In Fig. 18, we plot the subhalo σ_{3D} for GRP1 to redshift four against σ_{3D} for particles. The subhalo velocity bias and σ_{3D} are each consistent with no redshift evolution.

3.5 Power-law cosmologies

In order to examine the effects of the power spectral slope index, n, we have simulated a single renormalized volume cluster with a range of values for n. Here, the initial density fluctuation power spectrum is given by $P \propto k^n$, normalized to $\sigma_8 = 1.0$ as in the ΛCDM simulations. We plot the subhalo VDF for the cluster with initial conditions given by $n = 0, -1, -2$ and -2.7 in Fig. 19. There is a clear and strong trend that steeper power spectra have less substructure. This is a direct result of the fact that the shallower spectra have more small-scale power relative to large-scale power than the steeper spectra. Additionally, subhaloes form earlier in cosmologies with flatter power spectra, and have higher characteristic densities and steeper density profiles (e.g. Reed et al. 2005), making them less vulnerable to disruption.

4 CONCLUSIONS

(i) A universal subhalo VDF independent of host mass and redshift: the subhalo follows the self-similar relation $dn/dv = (1/8)(v_{cmax}/v_{cmax,host})^{-4}$ with a factor of 2 to 4 scatter.

(ii) Subhalo spins decrease towards the host centre. The radial dependence of subhalo spins is likely explained by the increased vulnerability of high-spin material to tidal stripping and disruption. Galaxies that form from low angular momentum subhaloes in high-density regions after some stripping has occurred would have a larger baryonic collapse factor. If we assume the size of the stellar distribution is proportional to λ (as in e.g. Kravtsov et al. 2004b), then stellar systems could be ∼50 per cent smaller if they form in heavily stripped central subhaloes. This would require that star formation continue after the subhalo has been stripped of high angular momentum material, as discussed previously. The circular velocity of the final stellar distribution could be lowered by a similar amount if the stars collapse to a small radius, assuming a central subhalo density slope near r^{-1} as found in simulations by Kazantzidis et al. (2004). Stoehr et al. (2002) proposed that the the apparent deficit of Local Group satellites could be explained if satellites actually reside in large subhaloes (further supported by Hayashi et al. 2003), which would allow the VDF of large Local Group satellites to match ΛCDM predictions. The small radii of the stellar distribution would give them low stellar velocity dispersion relative to v_{cmax} of their dark matter subhalo hosts. Baryonic spins of $\lambda < 0.01$ would be required for the gas to collapse to the required ∼1 per cent of the pre-stripped virial radius of the dark subhalo (Kazantzidis et al. 2004) needed to match Local Group satellites with ΛCDM predictions. However, only ∼5 per cent of our subhaloes have spins of $\lambda \lesssim 0.01$ and 90 per cent have $\lambda > 0.014$, so such a solution appears unlikely if the steep central substructure density profiles found by Kazantzidis et al. are correct.

(iii) Evidence for redshift dependence of the VDF: the shape and amplitude of the subhalo VDF has little or no trend with mass or redshift. However, fewer subhaloes lie at large $v_{\rm cmax}/v_{\rm cmax,host}$ in high-redshift hosts. This implies that dark matter haloes are not populated with large subhaloes until lower redshifts.

(iv) Could the VDF be a function of M/M_*? Though our data is consistent with only a weak or no trend of the VDF on host mass and redshift, a trend of less substructure in large M/M_* haloes would not be surprising, although it remains somewhat speculative until simulations are able to probe a larger mass and redshift range. The subhalo population approximately follows some fraction of the universal halo population. Thus, at large M/M_*, where the mass function is steep, the subhalo mass function should also be steep. The reason we see no such trend among redshift zero haloes in our sample may be because M/M_* for our simulated haloes is never much larger than unity, below which the slope of the field mass function has little mass dependence.

A dependence of substructure internal density profiles on M/M_* could also cause a trend for large M/M_* hosts to have decreased substructure. Virialized haloes have density profiles that become less centrally concentrated with increasing M/M_* (see e.g. Reed et al. 2005), so subhalo density profiles are likely to have a similar dependence. The lower central densities of low M/M_* subhaloes should make them more vulnerable to stripping and major disruption during and after virialization, even though their hosts also have lower central densities. The potential decrease in substructure at large M/M_* may be manifested in our highest redshift data (Fig. 5) where $M/M_* \sim 1000$. We note however that our power-law cosmology shows that the substructure abundance is also strongly dependent on the spectral slope. The fact that low-mass haloes sample steeper portions of the density power spectrum might cancel out any substructure dependence on M/M_*, though the range of spectral slopes present over our halo mass range is quite small. Also, because low-mass haloes generally form earlier, one might expect them to have less substructure because their subhaloes have been subject to tidal stripping and disruption for longer periods of time.

(v) Is there a central subhalo antibias? The slope of the subhalo number density is marginally consistent with that of the mass density for $r \gtrsim 0.3 r_{\rm vir}$, although a subhalo distribution that is shallower than the dark matter profile is favoured. More high-resolution simulations are needed to conclusively demonstrate a subhalo antibias at large radii. At smaller radii, subhaloes are deficient, but artificial numerical effects cannot be excluded. It is not surprising that more tidal stripping has occurred for subhaloes at small host radii, as reflected in the mass–radius trend of Fig. 14 and seen also by e.g. Gao et al. (2004a). One would also expect that the removal of sufficiently large masses would lead to a radial trend in $v_{\rm cmax}$, although such a radial trend may be masked by the preferential destruction of low $v_{\rm cmax}$ haloes at small radii in our results. In any case, because subhaloes are likely to have steep cuspy density profiles down to less than 1 per cent $r_{\rm vir}$ upon initial infall, as suggested by numerous studies of the density profiles of virialized haloes (e.g. Reed et al. 2005), then their centres will be highly resistant to tidal disruption. Thus, any appearance of subhalo antibias in current generation simulations is likely to be simply a manifestation of a radial trend in subhalo mass (or $v_{\rm cmax}$). The imposition of an arbitrary minimum mass (or minimum $v_{\rm cmax}$) as required by resolution constraints can give the false impression of missing central subhaloes (see also Gao et al. 2004b for a detailed discussion).

(vi) Subhaloes have no strongly preferred orbits. Orbital properties show no strong trends with respect to radius, redshift, or $v_{\rm cmax}$. However, the subhaloes on the most highly eccentric orbits become less abundant over time, likely as a result of disruption or heavy stripping by the central potential of the host, but this only affects a small fraction of total subhaloes. Subhaloes with small apocentres are most strongly affected. This likely has an artificial numerical cause wherein tidally affected subhaloes either lose enough material that they drop below resolution constraints, or are completely disrupted as a result of the effective density ceiling imposed upon simulated subhaloes. Our results also suggest that subhaloes have a positive velocity bias at small radii and little or no velocity bias at large radii. It is not clear how the addition of baryons in the form of gas and stars would affect orbital kinematics and distribution of the subhalo population.

(vii) Cosmological variance is too small to account for missing satellites. The subhalo VDF has a halo to halo cosmological variance of a factor of roughly 2 to 4. This means that the apparent problem of overpredicted Local Group satellites cannot be solved by invoking cosmological variance.

ACKNOWLEDGMENTS

We would like to thank the referee for insightful suggestions, which have improved this work. We thank Lucio Mayer for assistance with one of the runs. We are grateful to Frank van den Bosch, Felix Stoehr and Stelios Kazantzidis for helpful suggestions upon reading a draft of this paper. DR has been supported by the NASA Graduate Student Researchers Program and by PPARC. FG is a David E. Brooks Research Fellow. FG was partially supported by NSF grant AST-0098557 at the University of Washington. TQ was partially supported by the National Science Foundation. Simulations were performed on the Origin 2000 at NCSA and NASA Ames, the IBM SP4 at the Arctic Region Supercomputing Centre (ARSC) and at CINECA (Bologna, Italy), the NASA Goddard HP/Compaq SC 45, and at the Pittsburgh Supercomputing Centre. We thank Chance Reschke for dedicated support of our computing resources, much of which were graciously donated by Intel.

REFERENCES

Aubert D., Pichon C., Colombi S., 2004, MNRAS, 352, 376
Bardeen J. M., Bond J. R., Kaiser N., Szalay A. S., 1986, ApJ, 305, 15
Barnes J. E., Efstathiou G., 1987, ApJ, 319, 575
Bennett C. L. et al., 2003, ApJS, 148, 1
Benson A., Lacey C., Baugh C., Cole S., Frenk C., 2002a, MNRAS, 333, 156
Benson A., Frenk C., Lacey C., Baugh C., Cole S., 2002b, MNRAS, 333, 177
Bentley J. L., 1975, Commun. ACM, 18(9), 509
van den Bosch F. C., Abel T., Croft R., Hernquist L., White S., 2002, ApJ, 576, 21
van den Bosch F., Yang X., Mo H., 2003, MNRAS, 340, 771
van den Bosch F., Norberg P., Mo H., Yang X., 2004, MNRAS, 352, 1302
Bullock J. S., Kravtsov A. V., Weinberg D. H., 2000, ApJ, 539, 517
Bullock J. S., Dekel A., Kolatt T., Kravtsov A., Klypin A., Porcianni C., Primack J., 2001, ApJ, 555, 240
Chiba M., 2002, ApJ, 565, 17
Cole S., Lacey C., 1996, MNRAS, 281, 716
Colin P., Klypin A., Kravtsov K., 2000, ApJ, 539, 561
Colin P., Klypin A., Valenzuela O., Gottlober S., 2004, ApJ, 612, 50
Dalal N., Kochanek C. S., 2002, ApJ, 572, 25
Davis M., Efstathiou G., Frenk C. S., White S. D. M., 1985, ApJ, 292, 381

De Lucia G., Kauffmann G., Springel V., White S. D. M., Lanzoni B., Stoehr F., Tormen G., Yoshida N., 2004, MNRAS, 348, 333
Desai V., Dalcanton J. J., Mayer L., Reed D. S., Quinn T., Governato F., 2004, MNRAS, 351, 265
Diemand J., Moore B., Stadel J., Kazantzidis S., 2004a, MNRAS, 348, 977
Diemand J., Moore B., Stadel J., 2004b, MNRAS, 352, 535
Eke V. R., Cole S., Frenk C. S., 1996, MNRAS, 282, 263
Font A. S., Navarro J. F., Stadel J., Quinn T., 2001, ApJ, 563, L1
Gao L., White S. D. M., Jenkins A., Stoehr F., Springel V., 2004a, MNRAS, 355, 819
Gao L., De Lucia G., White S. D. M., Jenkins A., 2004b, MNRAS, L1
Gardner J. P., 2001, ApJ, 557, 616
Ghigna S., Moore B., Governato F., Lake G., Quinn T., Stadel J., 1998, MNRAS, 300, 146
Ghigna S., Moore B., Governato F., Lake G., Quinn T., Stadel J., 2000, 544, 616
Gill P., Knebe A., Gibson B., Dopita M., 2004, MNRAS, 351, 410
Gill P., Knebe A., Gibson B., 2004a, MNRAS, 351, 399
Gill P., Knebe A., Gibson B., 2005, MNRAS, 356, 1327
Gnedin O., 2003, ApJ, 582, 141
Goto T., Yamauchi C., Fujita Y., Okamura S., Sekiguchi M., Smail I., Bernardi M., Gomez P., 2003, MNRAS, 346, 601
Hayashi E., Navarro J., Taylor J., Stadel J., Quinn, T., 2003, ApJ, 584, 541
Katz N., White S., 1993, ApJ, 412, 478
Kazantzidis S., Mayer L., Mastropietro C., Diemand J., Stadel J., Moore B., 2004, ApJ, 608, 663
Klypin A., Kravtsov A., Valenzuela O., Prada F., 1999, ApJ, 522, 82
Kravtsov A., Berlund A., Wechsler R., Klypin A., Gottlober S., Allgood B., Primack J., 2004a, ApJ, 609, 35
Kravtsov A., Gnedin O., Klypin A., 2004b, ApJ, 609, 482
Lacey C., Cole S., 1994, MNRAS, 271, 676
Lemson G., Kauffmann G., 1999, MNRAS, 302, 111
Mao S., Schneider P., 1998, MNRAS, 295, 587
Mao S., Jing Y., Ostriker J., Weller J., 2004, ApJ, 604, L5
Mayer L., Governato F., Colpi M., Moore B., Quinn T., Wadsley J., Stadel J., Lake G., 2001, ApJ, 547, L123
Metcalf R., Madau P., 2001, ApJ, 563, 9
Mo H., Mao S., White S. D. M., 1998, MNRAS, 295, 319
Moore B., Katz N., Lake G., 1996, ApJ, 457, 455
Moore B., Governato F., Quinn T., Stadel J., Lake G., 1998, AJ, 499, L5
Moore B., Ghigna S., Governato F., Lake G., Quinn T., Stadel J., Tozzi P., 1999, ApJ, 524, L19
Nagai D., Kravtsov A., 2005, ApJ, 618, 557
Peebles J., 1969, ApJ, 155, 393
Peirani S., Mohayaee R., Pacheco J., 2004, MNRAS, 348, 921
Power C., Navarro J. F., Jenkins A., Frenk C. S., White S. D. M., Springel V., Stadal J., Quinn T., 2003, MNRAS, 338, 14
Press W. H., Davis M., 1982, ApJ, 259, 449
Press W. H., Schechter P., 1974, ApJ, 187, 425
Reed D., Gardner J., Quinn T., Stadel J., Fardal M., Lake G., Governato F., 2003a, MNRAS, 346, 565
Reed D., Governato F., Verde L., Gardner J., Quinn T., Merritt D., Stadel J., Lake G., 2005, MNRAS, 357, 82
Ryden B. S., 1988, ApJ, 329, 589
Sheth R. K., Tormen G., 1999, MNRAS, 308, 119
Somerville R., 2002, ApJ, 572, L23
Spergel D. et al., 2003, ApJS, 148, 175
Springel V., White S. D. M., Tormen G., Kauffmann G., 2001, MNRAS, 328, 726
Stadel J., 2001, PhD thesis, Univ. Washington
Stoehr F., White S. D. M., Tormen G., Springel V., 2002, MNRAS, 335, 84
Stoehr F., White S. D. M., Springel V., Tormen G., Yoshida N., 2003, MNRAS, 345, 1313
Syer D., White S. D. M., 1998, MNRAS, 293, 337
Taffoni G., Mayer L., Colpi M., Governato F., 2003, 341, 434
Taylor J., Babul A., 2004, MNRAS, 348, 811
Tormen G., Diaferio A., Syer D., 1998, MNRAS, 299, 728
Vale A., Ostriker J., 2004, MNRAS, 353, 189
Verde L., Oh S. Peng, Jimenez R., 2002, MNRAS, 336, 541
Vitvitska M., Klypin A., Kravtsov A., Wechsler R., Primack J., Bullock J., 2002, ApJ, 581, 799
Wadsley J., Stadel J., Quinn T., 2004, New Astron., 9, 137
Warren M., Quinn P., Salmon J., Zurek W., 1992 ApJ, 399, 405
White S. D. M., Rees M. J., 1978, MNRAS, 183, 341
Whitmore B., Gilmore D., 1991, ApJ, 367, 64
Willman B., Governato F., Dalcanton J., Reed D., Quinn T., 2004, MNRAS, 353, 639
Yang X., Mo H., van den Bosch F., 2003, MNRAS, 339, 1057

This paper has been typeset from a TEX/LATEX file prepared by the author.